A study of helium bubble production in 10 keV He+ irradiated tungsten

Xiaoou Yi [a,*], Kazuto Arakawa [b], Duc Nguyen-Manh [c], Francesco Ferroni [d], Pingping Liu [a], Wentuo Han [a], Farong Wan [a], Steven G Roberts [c,d]

[a] School of Materials Science and Engineering, University of Science and Technology Beijing, Beijing, 100083, China
[b] Department of Materials Science, Faculty of Science and Engineering, Shimane University, 1060 Nishikawatsu, Matsue, 690-8504, Japan
[c] CCFE, Culham Science Centre, Abingdon, OX14 3DB, UK
[d] Department of Materials, University of Oxford, Parks Road, OX1 3PH, Oxford, UK

HIGHLIGHTS

- TEM observation of helium bubbles in tungsten required a threshold fluence of $\sim 4.5 \times 10^{19}$ He+/m^2 (He-peak: 10,800 appm).
- Temperature has a pronounced impact on bubble size and population. At $T \geq 1273$ K, 1D-alignment of bubbles was observed, suggesting a small degree of spatial ordering.
- Helium fluence exhibited limited impact on bubble size at $T < 1473$ K. At 1473 K, bubble growth became remarkably enhanced by the increase of helium fluence, while the bubble population remained almost constant.
- During high temperature equilibrium, the average configuration of helium-vacancy complexes is $He_{3m}V_m$ ($m \geq 1$).

ARTICLE INFO

ABSTRACT

Helium bubble production in tungsten has been studied combining transmission electron microscopy and *in situ* irradiations with 10 keV He+ ions. The irradiations were carried out at four temperatures (773 K, 1073 K, 1273 K, 1473 K), and were held at intervals of $(0.45; 0.9; 1.2; 1.5) \times 10^{20}$ He+/m^2 for each temperature. Based on detailed analyses of bubble size, population and spatial distributions, their correlations with irradiation temperature and helium fluence were established. Helium-to-vacancy ratios were also deduced from these data. During high temperature equilibrium, the ratio was close to 3.

© 2017 Elsevier B.V. All rights reserved.

1. Introduction

Tungsten-based materials form a prime candidate of plasma facing components (PFC) in fusion power reactors. During reactor operation, they will be subject to bombardments of 14 MeV neutrons, as well as the deposition of high concentrations of helium and hydrogen isotopes. This gives rise to material degradations including radiation-hardening, swelling, surface roughening, intergranular and transgranular embrittlement [1]. The presence of helium tends to enhance these processes by shaping the evolution of radiation-induced damage microstructure. Iwakiri et al. [2] investigated the role of helium in this regard based on *in situ* observations of microstructure in 0.25 keV and 8 keV He+ irradiated tungsten. The maximum transferred kinetic energy from these He+ ions are estimated to be ~ 21 eV and ~ 667 eV, respectively, in correspondence with sub-threshold (<90 eV) and above-threshold (>90 eV) damage in tungsten [3]. The authors have successfully established the correlations between temperature (293, 873, 1073 K), helium fluence ($10^{18} - 10^{21}$ He/m^2) and damage microstructure. The changes of mechanical properties were reported in Yoshida et al. [4].

In the present study, we wish to expand the investigated temperature range to 1473 K, which is relevant to the standard operating temperature of tungsten divertors [5]. The production of helium bubbles in 10 keV He+ (above-threshold) irradiations of tungsten will be studied *in situ*. Detailed transmission electron microscopy will reveal the relationship between helium bubble characteristics (size, population, spatial distribution), irradiation temperature and helium fluence. In particular, a statistical approach will be performed in order to deduce the average

---
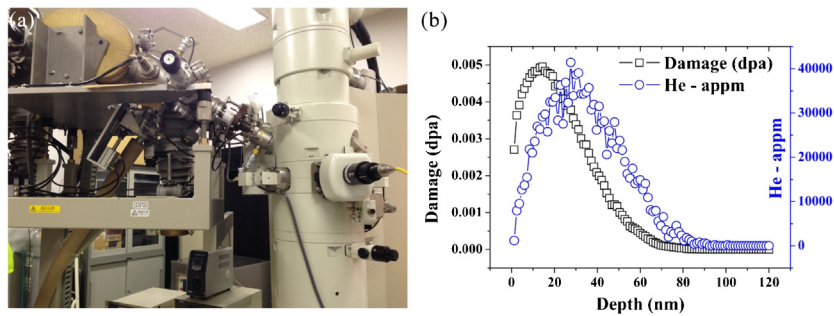
Fig. 1. a) Side view of the *in situ* irradiation facility at Shimane University; b) SRIM profiles of displacement damage and helium concentration for 10 keV He$^+$ irradiations in tungsten, at a fluence of 1.5×10^{20} He$^+$/m^2.

Table 1
Summary of irradiation conditions.

	Temp. (K)	Fluence ($\times 10^{20}$ He$^+$/m^2)	[a]He-peak (appm)	[a]dpa
W	773	0.45	10,800	0.0011
	1073	0.9	21,600	0.0022
	1273	1.2	28,800	0.0030
	1473	(1.35)	(32,400)	(0.0033)
		1.5	36,000	0.0037

[a] Average was taken over a 10 nm depth range near the peak helium concentration and the peak damage region, respectively.

configuration of helium-vacancy complexes in tungsten (i.e. the He/V-ratio), as a function of temperature and helium fluence. The formation of helium-vacancy complexes may serve as diffusion barriers for injected helium from the plasma, and weaken the detrimental effects of blistering, exfoliation and material embrittlement. This work on He/V-ratios is unprecedented for tungsten, yet crucial in understanding the transport of helium in tungsten, and how it is associated with the configuration of helium-vacancy complexes.

2. Experimental

Thin sheets of polycrystalline tungsten (typically >99.996 wt%) were sourced from Plansee Gruppe, Austria, with the following traces of impurities present: C, <10 ppm; P, < 10 ppm; Si and O, ~5 ppm by weight. 3 mm TEM discs were punched from the material, mechanically thinned to ~ 80 μm, heat treated in vacuum at 1673 K for 20 h, and electropolished in 0.5 wt% NaOH aqueous solution. The resulting grain size exceeded 100 μm on average.

In situ irradiations were carried out on a JEOL 2010 incorporated with a low energy ion accelerator at Shimane University (Fig. 1a). 10 keV He$^+$ ions were diverted towards the thin-foil normal at an incident angle of ~17° from the vertical direction and a flux of 5×10^{16} He$^+$/m^2/s. The sample temperature was measured to within ± 5 K using Cr-Al thermocouple wires attached to the Ta-furnace. Electron microscopy was carried out at intervals of (0.45; 0.9; 1.2; 1.5) $\times 10^{20}$ He$^+$/m^2. Samples were mounted in a Gatan 628.TA single-tilt heating holder and a total of four temperatures (773, 1073, 1273 and 1473 K) were investigated, respectively.

Depth profiles of displacement damage and helium concentration for 10 keV He$^+$ ions were calculated from SRIM 2013. 10,000 ions were run using the "Quick" Kinchin-Pease option. The displacement threshold energy and the lattice binding energy of tungsten were set to 90 eV and 0, respectively [3,6]. Results in correspondence with the final fluence of 1.5×10^{20} He$^+$/m^2 are shown in Fig. 1b. All experiment conditions are summarized in Table. 1. Average was taken over a 10 nm depth range near the peak helium concentration and peak displacement damage zone, respectively.
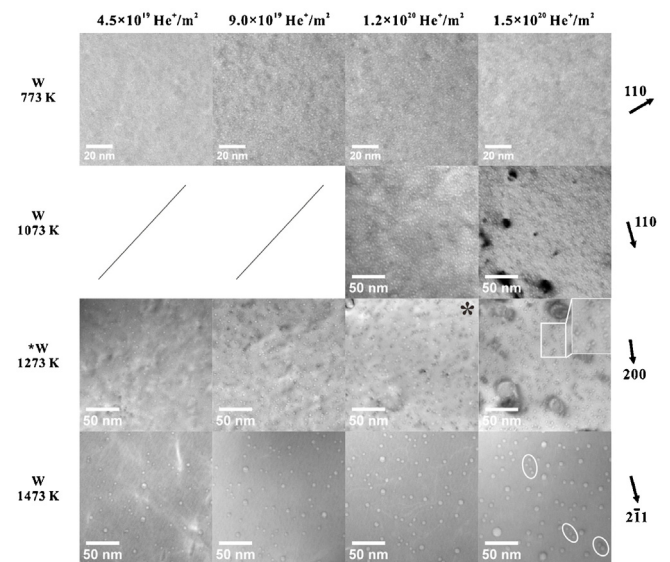

Fig. 2. Bubble production in tungsten as a function of irradiation temperature and helium fluence. All micrographs shown were recorded with $\Delta f = -1331$ nm. The micrograph marked with '*' corresponds to 1.35×10^{20} He$^+$/m^2. Regions labelled with white box and circle demonstrate evidence of bubble ordering.

3. Results and discussion

3.1. Damage microstructure

Damage microstructure in 10 keV He$^+$ ion irradiated tungsten was foil-thickness-dependent. In this study, the characterization of helium bubbles was focus on thin regions with foil thickness < 100 nm. Strong surface sinks were present, effectively eliminating the radiation-induced SIAs and clusters, and leaving behind the vacancies. In thicker regions, both dislocations and helium bubbles were observed. Dislocation loops and line entanglements were frequently found decorated with bubbles. Thick region microstructures and dislocation-bubble interactions will be discussed in another paper.

Fig. 2 illustrates the production of helium bubbles in tungsten, as a function of irradiation temperature (773–1473 K) and helium fluence (0.45 – 1.5) $\times 10^{20}$ He$^+$/m^2. The micrographs shown were all recorded in under-focus condition with $\Delta f = -1331$ nm. The grain orientations were close to z = ⟨001⟩ for T < 1473 K and close to z = ⟨113⟩ for T = 1473 K. A threshold fluence of ~4.5×10^{19} He$^+$/m^2 was found for observing bubbles. At T = 773 K and 1073 K, the bubbles were mostly <4.5 nm in diameter and randomly distributed. At T ≥ 1273 K, 1D-alignment of bubbles was observed, suggesting a small degree of spatial ordering. The direction of bubble alignment has been found//⟨100⟩ at 1273 K and close to//⟨211⟩ at 1473 K.
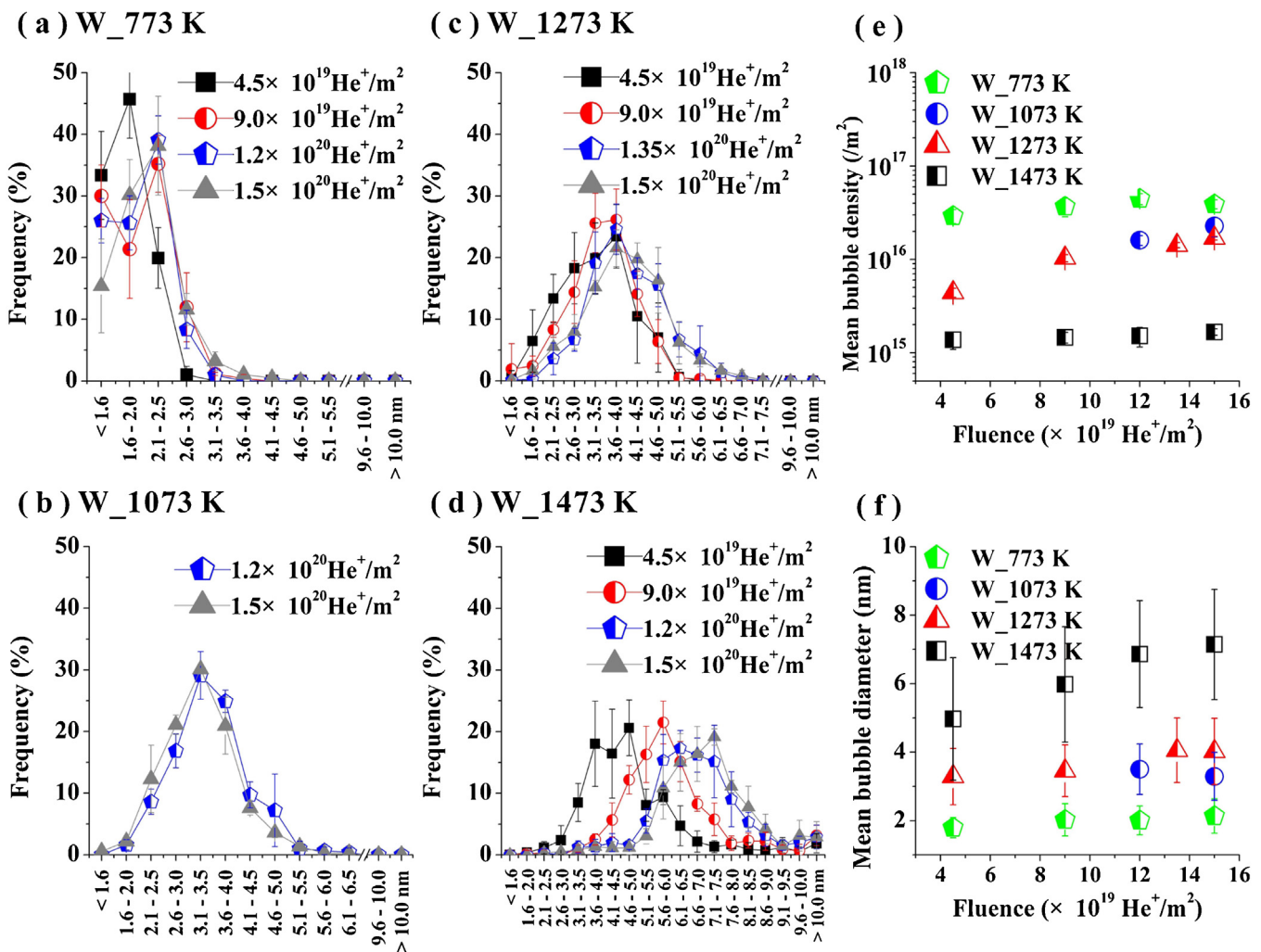
Fig. 3. a–d) Bubble size distributions at 773 K, 1073 K, 1273 K and 1473 K. Mean bubble density and mean bubble diameter are shown as a function of temperature and helium fluence in e) and f), respectively.

Owing to the absence of large SIA-type clusters and dislocations in the microstructure, we suspected the possible cause of bubble decoration of loops. Instead, the bubbles were found associated with strain fields in weak-beam dark-field micrographs. This suggested that the bubbles were pressurized and the elastic strain might have facilitated the short-range ordering observed. At $T \geq 1273$ K, distinct growth of bubbles also took place, whilst the bubble population encountered a sharp fall. The increase of helium fluence also favoured the growth of bubbles. At $T = 1473$ K, the largest bubble size exceeded 16 nm in diameter, at the final fluence of 1.5×10^{20} He$^+$/m^2.

3.2. Evolution of bubble size and population

Fig. 3a–d) show bubble size (diameter) distributions averaged over several images in tungsten, as a function of irradiation temperature and helium fluence. Mean bubble densities and mean bubble diameters are shown in Fig. 3e) and f), respectively. The overall sampling body was around 100 for each data point, demonstrating the trends of bubble size and population evolution with good statistical significance.

At 773 K, over 95% of helium bubbles were less than 3 nm in diameter. Mean bubble density almost saturated as early as 4.5×10^{19} He$^+$/m^2, and measured around $(3.0 - 4.0) \times 10^{16}$/m^2. The increase of helium fluence showed subtle impact in bubble growth.

A small increase in mean bubble size was found from ~2.0 nm to ~3.5 nm, when increasing the temperature to 1073 K. The largest bubble size shifted from 4.5 nm to 6.5 nm. Over 95% of bubbles were still under 5 nm in diameter. Mean bubble density dropped by a factor of 2. Similarly, the increase of helium fluence showed negligible impact.

At 1273 K, the mean bubble size increased to ~4 nm and the largest bubble size shifted to ~7.5 nm. Helium fluence played an important role in the evolution of bubble population, but not so much for the bubble size. Mean bubble density increased from ~4.4×10^{15}/m^2 to ~1.7×10^{16}/m^2, when the helium fluence accumulated from 4.5×10^{19} He$^+$/m^2 to 1.5×10^{20} He$^+$/m^2.

At 1473 K, mean bubble diameter at the low fluence of 4.5×10^{19} He$^+$/m^2 exceeded 5 nm. This was a remarkable increase by a factor of 2.5, compared with 773 K. Meanwhile, bubble density at this fluence was over an order of magnitude lower than that of 773 K. Further increase in helium fluence resulted in subtle change in bubble population, but notably favoured the growth of bubbles, to ~7.1 nm in mean bubble diameter. About 3% of the total bubble population exceeded 10 nm in diameter.

3.3. Helium-to-vacancy ratio

Helium-to-vacancy ratios were obtained assuming that all implanted helium resided in visible bubbles. A backscattering prob-
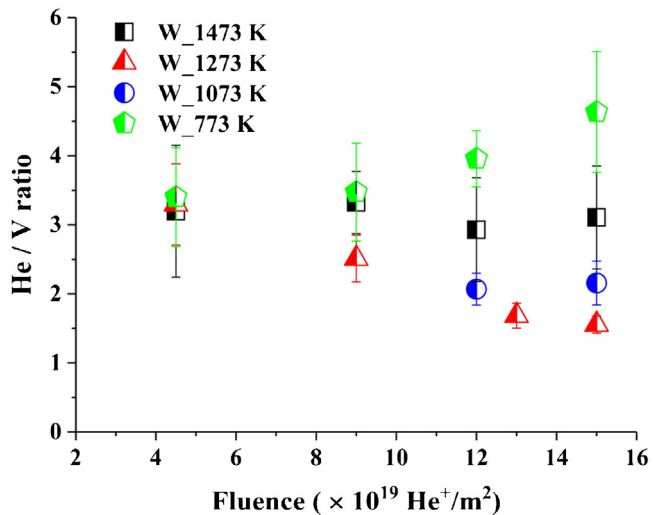
Fig. 4. He/V-ratio in tungsten, plotted as a function of irradiation temperature and helium fluence.

ability of 0.30 ± 0.01 was found from SRIM 2013, and this loss of helium has been taken into account in the calculation of the total amount of helium atoms. All bubble geometries were regarded as ideal spheres. The volume of a vacancy in tungsten was taken from DFT data in Ref. [7], i.e. $\Omega = \Omega_0 - 0.37\,\Omega_0 = 0.63\,\Omega_0$, where $\Omega_0 = 15.85\,\text{Å}^3$ and represents the perfect atomic volume of tungsten at 298 K. Finding the ratio between the total measured volume of observed bubbles and Ω gave the total amount of vacancies. The amount of volume relaxation $-0.37\,\Omega_0$ corresponds to that of a monovacancy. Effects of volume relaxation in di-vacancies and tri-vacancies upon results of He/V-ratios have also been evaluated. According to Ref. [7], the fraction of volume which a single vacancy takes up in a di-vacancy (1NN) and a tri-vacancy (1NN(2)+2NN) configuration can be written as: $(2\,\Omega_0 - 0.72\,\Omega_0)/2 = 0.64\,\Omega_0$ and $(3\,\Omega_0 - 1.08\,\Omega_0)/3 = 0.64\,\Omega_0$, respectively. Essentially, this introduces subtle difference on the results of He/V-ratio. Hence, all He/V-ratios deduced from this work have adopted the monovacancy assumption for treating volume relaxation effect. The results are summarized in Fig. 4 and plotted as a function of irradiation temperature and helium fluence.

When helium fluence was low, the He/V-ratio remained constant between 3 and 3.5, independent of irradiation temperature. At higher fluences, the values of He/V-ratios diverged. At 773 K, helium bubble population appeared saturated with increasing fluence whilst the growth of these bubbles appeared subtle. This has led to the remarkable increase of He/V-ratio towards $\sim$4.6. At 1073 K and 1273 K, helium bubble population increased with increasing fluence, while the size of bubbles remained nearly constant. This has pulled down the He/V-ratio to $1.5 - 2.5$. At 1473 K, the population of helium bubbles remained almost constant with the increase of helium fluence, but each existing bubble encountered substantial amount of growth. The resulting He/V-ratio varied at around 3.

This statistical approach in deducing He/V-ratios from TEM micrographs has its limitations, since not all helium-vacancy complexes were necessarily within the resolution limit of phase-contrast imaging. Owing to this limit, all bubbles considered in this method were >1 nm in diameter. However, one may safely argue that for high temperature irradiations such as 1473 K, thermal equilibrium of radiation defects can be achieved within short intervals and all retained helium were accommodated within visible bubbles. It follows that under these circumstances, the most stable configuration of helium-vacancy complex is He_{3m}V_m ($m \geq 1$).

Recent results of density functional calculations (DFT) are in good agreement with this finding [8]. A joint experiment-modelling paper on this topic is in preparation.

4. Conclusions

A study of helium bubble production has been carried out in pure tungsten, resulting from in-situ 10 keV He$^+$ ion irradiations. Detailed defect characterizations demonstrated the effect of irradiation temperature and helium fluence. It is found that:

1) TEM observation of helium bubbles in tungsten required a threshold fluence of $\sim$$4.5 \times 10^{19}$ He$^+$/m^2 for all temperatures investigated.
2) Temperature had a pronounced impact on bubble size and population. At $T \geq 1273$ K, 1D-alignment of bubbles was observed, suggesting a small degree of spatial ordering.
3) Helium fluence exhibited limited impact on bubble size at $T < 1473$ K. Meanwhile, the population of bubbles generally increased with increasing fluence. At 1473 K, bubble growth became remarkably enhanced by the increase of helium fluence, while the bubble population remained almost constant.
4) The average configurations of helium-vacancy complexes were determined from the He/V- ratios, as a function of temperature and helium fluence. During high temperature equilibrium, the ratio was found close to 3.

References

[1] Y. Watanabe, H. Iwakiri, N. Yoshida, et al., Formation of interstitial loops in tungsten under helium ion irradiation: rate theory modeling and experiment, Nucl. Instrum. Methods Phys. Res. B 255 (2007) 32–36.
[2] H. Iwakiri, K. Yasunaga, K. Morishita, et al., Microstructure evolution in tungsten during low-energy helium ion irradiation, J. Nucl. Mater. 283–287 (2000) 1134–1138.
[3] Standard practice for neutron radiation damage simulation by charged-particle irradiation, ASTM, International, Designation: E 521-96 (Reapproved 2003).
[4] N. Yoshida, H. Iwakiri, K. Tokunaga, et al., Impact of low energy helium irradiation on plasma facing metals, J. Nucl. Mater. 337–339 (2005) 946–950.
[5] V. Barabash, G. Federici, J. Linke, et al., Material/plasma surface interaction issues following neutron damage, J. Nucl. Mater. 313–316 (2003) 42–51.
[6] R.E. Stoller, M.B. Toloczko, G.S. Was, et al., On the use of SRIM for computing radiation damage exposure, Nucl. Instrum. Methods Phys. Res. B 310 (2013) 75–80.
[7] F. Hofmann, D. Nguyen-Manh, M.R. Gilbert, et al., Lattice swelling and modulus change in a helium-implanted tungsten alloy: x-ray micro-diffraction, surface acoustic wave measurements, and multiscale modeling, Acta Mater. 89 (2015) 352–363.
[8] D. Nguyen-Manh, S.L. Dudarev, Trapping of He clusters by inert-gas impurities in tungsten: first-principles predictions and experimental validation, Nucl. Instrum. Methods Phys. Res. B. 352 (2015) 86–91.